AFRL-RX-WP-JA-2017-0352

WORK FUNCTION CHARACTERIZATION OF DIRECTIONALLY SOLIDIFIED LAB6–VB2 EUTECTIC (POSTPRINT)

Steven B. Fairchild and John J. Boeckl
AFRL/RX

Tyson C. Back
University of Dayton Research Institute

Andreas K. Schmid Floor Derkink, and Chen Gong
Lawrence Berkeley National Laboratory

Marc Cahay
University of Cincinnati

Ali Sayir
NASA Glenn Research Center

28 April 2017
Interim Report

AIR FORCE RESEARCH LABORATORY
MATERIALS AND MANUFACTURING DIRECTORATE
WRIGHT-PATTERSON AIR FORCE BASE, OH 45433-7750
AIR FORCE MATERIEL COMMAND
UNITED STATES AIR FORCE

REPORT DOCUMENTATION PAGE

Form Approved
OMB No. 0704-0188

1. REPORT DATE *(DD-MM-YY)*	2. REPORT TYPE	3. DATES COVERED *(From - To)*
28 April 2017	Interim	6 May 2010 – 30 September 2016

4. TITLE AND SUBTITLE
WORK FUNCTION CHARACTERIZATION OF DIRECTIONALLY SOLIDIFIED LAB6–VB2 EUTECTIC (POSTPRINT)

5a. CONTRACT NUMBER
IN-HOUSE

5b. GRANT NUMBER

5c. PROGRAM ELEMENT NUMBER

6. AUTHOR(S)
1) Steven B. Fairchild and John J. Boeckl – AFRL/RX
2) Tyson C. Back – UDRI
(continued on page 2)

5d. PROJECT NUMBER

5e. TASK NUMBER

5f. WORK UNIT NUMBER
X09X

7. PERFORMING ORGANIZATION NAME(S) AND ADDRESS(ES)
1) AFRL/RX
Wright-Patterson AFB, OH 45433
2) University of Dayton Research Institute
300 College Park Ave.
Dayton, OH 45469
(continued on page 2)

8. PERFORMING ORGANIZATION REPORT NUMBER

9. SPONSORING/MONITORING AGENCY NAME(S) AND ADDRESS(ES)
Air Force Research Laboratory
Materials and Manufacturing Directorate
Wright-Patterson Air Force Base, OH 45433-7750
Air Force Materiel Command
United States Air Force

10. SPONSORING/MONITORING AGENCY ACRONYM(S)
AFRL/RXAP

11. SPONSORING/MONITORING AGENCY REPORT NUMBER(S)
AFRL-RX-WP-JA-2017-0352

12. DISTRIBUTION/AVAILABILITY STATEMENT
Distribution Statement A. Approved for public release: distribution unlimited.

13. SUPPLEMENTARY NOTES
PA Case Number: 88ABW-2017-2091; Clearance Date: 28 Apr 2017. This document contains color. Journal article published in Ultramicroscopy, 10 May 2017. © 2017 Elsevier B.V. The U.S. Government is joint author of the work and has the right to use, modify, reproduce, release, perform, display, or disclose the work.
The final publication is available at www.elsevier.com/locate/ultramic http://dx.doi.org/10.1016/j.ultramic.2017.05.006

14. ABSTRACT *(Maximum 200 words)*
With its low work function and high mechanical strength, the LaB_6 /VB_2 eutectic system is an interesting candidate for high performance thermionic emitters. For the development of device applications, itis important to understand the origin, value, and spatial distribution of the work function in this system. Here we combine thermal emission electron microscopy and low energy electron microscopy with Augerelectron spectroscopy and physical vapor deposition of the constituent elements to explore physical and chemical conditions governing the work function of these surfaces. Our results include the observation that work function is lower (and emission intensity is higher) on VB_2 inclusions than on the La B_6 matrix. We also observe that the deposition of atomic monolayer doses of vanadium results in surprisingly significant lowering of the work function with values as low as 1.1 eV.

15. SUBJECT TERMS
LaB_6 /VB_2; eutectic; thermionic emitter; thermal emission electron microscopy; Augerelectron spectroscopy; vapor deposition

16. SECURITY CLASSIFICATION OF:			17. LIMITATION OF ABSTRACT:	18. NUMBER OF PAGES	19a. NAME OF RESPONSIBLE PERSON (Monitor)
a. REPORT	b. ABSTRACT	c. THIS PAGE			Steven Fairchild
Unclassified	Unclassified	Unclassified	SAR	8	19b. TELEPHONE NUMBER *(Include Area Code)* (937) 904-4328

REPORT DOCUMENTATION PAGE Cont'd

6. AUTHOR(S)

3) Andreas K. Schmid Floor Derkink, and Chen Gong - LBNL

4) Marc Cahay - University of Cincinnati

5) Ali Sayir - NASA Glenn Research Center

7. PERFORMING ORGANIZATION NAME(S) AND ADDRESS(ES)

3) Lawrence Berkeley National Laboratory
1 Cyclotron Rd, Berkeley, CA 94720

4) University of Cincinnati, 2600 Clifton Ave.
Cincinnati, Ohio, 45221-003

5) NASA Glenn Research Ctr, 21000 Brookpark Rd.
Cleveland, OH 44135

Ultramicroscopy 000 (2017) 1–5

Contents lists available at ScienceDirect

Ultramicroscopy

journal homepage: www.elsevier.com/locate/ultramic

Work function characterization of directionally solidified LaB_6–VB_2 eutectic

Tyson C. Back[a,b,*], Andreas K. Schmid[c], Steven B. Fairchild[b], John J. Boeckl[b], Marc Cahay[d], Floor Derkink[c,e], Gong Chen[c], Ali Sayir[f]

[a] University of Dayton Research Institute, 300 College Park, Dayton, OH 45469-0170, USA
[b] Air Force Research Laboratory, Materials and Manufacturing Directorate, 3005 Hobson Way, Wright-Patterson Air Force Base, OH 45433, USA
[c] NCEM, Molecular Foundry, Lawrence Berkeley National Laboratory, Berkeley, CA 94720, USA
[d] Spintronics and Vacuum Nanoelectronics Laboratory, University of Cincinnati, Cincinnati, OH 45221, USA
[e] Physics of Interfaces and Nanomaterials, MESA+ Institute for Nanotechnology, University of Twente, P.O. Box 217, 7500 AE, Enschede, The Netherlands
[f] NASA Glenn Research Center, Cleveland, OH 44135, USA

ARTICLE INFO

Article history:
Received 30 December 2016
Revised 11 April 2017
Accepted 9 May 2017
Available online xxx

ABSTRACT

With its low work function and high mechanical strength, the LaB_6/VB_2 eutectic system is an interesting candidate for high performance thermionic emitters. For the development of device applications, it is important to understand the origin, value, and spatial distribution of the work function in this system. Here we combine thermal emission electron microscopy and low energy electron microscopy with Auger electron spectroscopy and physical vapor deposition of the constituent elements to explore physical and chemical conditions governing the work function of these surfaces. Our results include the observation that work function is lower (and emission intensity is higher) on VB_2 inclusions than on the LaB_6 matrix. We also observe that the deposition of atomic monolayer doses of vanadium results in surprisingly significant lowering of the work function with values as low as 1.1 eV.

1. Introduction

LaB_6 has been used as thermionic emitter for several decades. It was recognized early on that LaB_6 had many properties that were beneficial for use as a cathode, such as low work function (2.7 eV) and lower operating temperatures (~1500 K) [1]. LaB_6 also has an energy spread roughly half that of tungsten under the same accelerating voltage [2]. All of which are an improvement over the standard tungsten electron sources with the main limiting factor to more widespread use being cost. As a result, LaB_6 has been employed in a wide variety of applications requiring an electron source, which include electron microscopes, traveling wave tubes, and Hall/ion thrusters.

Directionally solidified eutectics consist of a two-phase material with one phase distributed throughout the matrix of the second phase. This class of materials have been shown to have desirable high-temperature mechanical properties compared to existing composites [3–9]. Somewhat more recently LaB_6 directionally solidified eutectic (DSE) materials have been shown to offer further mechanical improvements over standard LaB_6 [10]. LaB_6 DSEs consist of a LaB_6 matrix phase with a transition metal di-boride phase that forms fibers homogenously throughout the matrix. Typical transition metals consist of Zr, Hf, Ti, and V. The improvement in mechanical properties is attributed to the interface between the two phases in the eutectic. Additionally, this material system has also shown significant improvements in thermionic emission current density when compared with standard single crystal LaB_6 [11, 12]. LaB_6/VB_2 was shown to have an order of magnitude improvement in current density when compared to single crystal LaB_6 [12].

The combination of high mechanical strength and current density make LaB_6 DSEs ideal candidates for use in applications where high power and long term stability are critical such as use in Hall/ion thrusters where cathode requirements up to 400 A and 10^4 h could be necessary [13]. Although previous electron emission studies of LaB_6 DSEs have shown significant improvements over existing thermionic cathodes, a fundamental understanding of why is lacking. It is the purpose of this paper to investigate dynamic changes in work function for LaB_6/VB_2 with low energy electron microscopy (LEEM). The thermionic electron emission microscopy (ThEEM) imaging mode and reflectivity curves were used to characterize the work function of the surface under stoichiometric and nonstoichiometric conditions.

* Corresponding author.
E-mail address: tyson.back@udri.udayton.edu (T.C. Back).

http://dx.doi.org/10.1016/j.ultramic.2017.05.006
0304-3991/

2. Experimental procedures

The LaB_6/VB_2 samples were directionally solidified by a zone melting technique previously described elsewhere [10]. The crystal growth resulted in cylindrical rods which were then cut and polished. After polishing the samples were transferred into a spin polarized low energy electron microscope (SPLEEM) at the National Center for Electron Microscopy at Lawrence Berkeley National Laboratory. Before imaging the samples were introduced into a sample preparation chamber for cleaning that consisted of Ar ion sputtering in a background of O_2, 3.0×10^{-8} Torr. During sputtering the sample was flashed to 1250 °C for 40 s with a final flash in vacuum. This was repeated multiple times until the sample surface was free of carbon and oxygen which was checked with Auger electron spectroscopy (AES). Once clean, the sample was transferred into the SPLEEM imaging chamber which maintained a base pressure of 2×10^{-11} Torr. All images were acquired in the bright field imaging mode. The SPLEEM setup has been described elsewhere [14,15].

In order to determine work function, a series of images were acquired by systematically changing the starting voltage on the sample to generate a reflectivity curve. The curves can be used to determine at what point the transition from mirror mode to scattering mode, sometimes referred to as the MEM-LEEM transition, occurred. This transition can be used to determine the work function of the sample surface using the relationship $\varphi_S = eV_{onset} + \varphi_G$, where φ_S is the work function of the sample in eV, V_{onset} is the threshold voltage in volts and φ_G is the effective work function of the electron gun [16–19]. In order to accurately determine the work function of the sample by this method the effective work function of the electron gun in the LEEM must be known. To accomplish this highly oriented pyrolytic graphite (HOPG) and W(1 1 0) were used for calibration. Reflectivity curves were acquired from these samples by collecting a series of images created by changing the starting voltage on the sample. To determine the work function from these curves several fitting methods are possible. Recently, Mathieu et al. [20] used a complementary error function (erfc) to obtain a work function value. This method worked well when transitions are sharp and energy resolution is high. However, for instances where the transition is broad the erfc fit tends to over-estimate the work function. The erfc fit is sensitive to the energy-width of the transition (for LEEM this is the transition from mirror mode to scattering) and broader distributions tend to yield higher work function values. Another previously used method [16–19] involves the use of two linear fits to determine work function from the intersection of these two lines. Although simple, it is found that this method is more consistent with work function determination reported elsewhere [16,21], particularly when the energy-width of the transition from mirror mode to scattering is relatively broad, a condition that exists in the data reported here. For calibration, the linear fit method was used to determine the work function of both W(1 1 0) and HOPG which was found to be 5.2 eV and 4.7 eV, respectively. These experimentally determined values agree well with values previously reported for W(1 1 0) [22–26] and HOPG [27–32]. Fig. 1 is a reflectivity curve from HOPG demonstrating the linear fit procedure. All work function values were corrected for Schottky barrier lowering of the work function due the field between the sample and the objective lens, which was estimated to 0.048 eV.

This intersection represents the transition from mirror mode into scattering mode. These curves were used to create a spatially resolved work function map. In order to characterize the effects of non-stoichiometric surfaces on work function the samples were dosed with monolayer (ML) coverages of La, V, and B separately during image acquisition. V and B were deposited by *e*-beam evaporation and La by thermal evaporation. For calibration of deposition rate each individual elemental component was deposited onto a clean LaB_6 surface. The deposition rate was determined by monitoring the image intensity oscillations that are consistent with atomic layer-by-layer growth. Samples were also imaged in thermal emission imaging mode or ThEEM. In ThEEM only thermally emitted electrons from the sample are used for imaging. In this imaging mode, thermionic emission curves were obtained by plotting the total intensity of the image as a function of temperature [33].

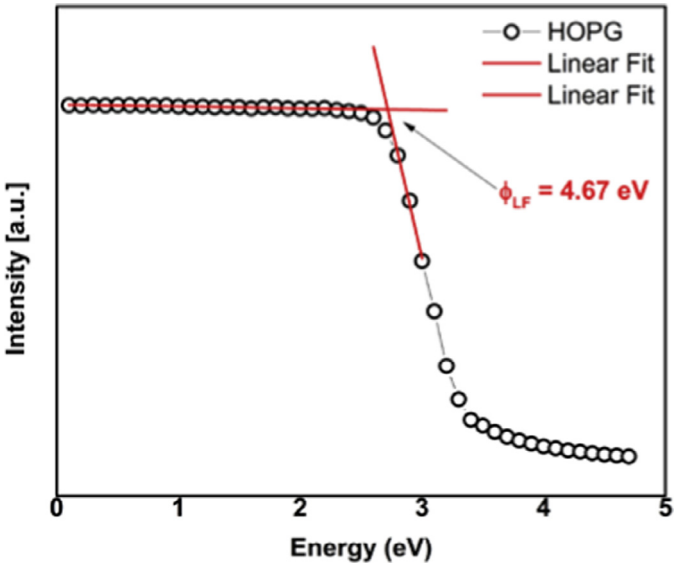

Fig. 1. Reflectivity curve from HOPG. Using the linear fit method resulted in a work function of 4.67 eV.

3. Results and discussion

It was previously shown thatLaB_6–MeB_2 (where Me = V, Zr, Ti, and Hf) materials exhibit significant improvements in thermal emission current density compared to pure LaB_6 [12]. It was found that for all the compositions tested it was the eutectic composition that always yielded the highest current density [34]. Of the transition metal di-borides tested, the VB_2 compound yielded the highest current density. Fig. 1 shows a LEEM image of the LaB_6/VB_2 surface. The dark areas in the image consist of circular features roughly 500 nm in diameter which are the VB_2 phase. The lighter areas in the image are the LaB_6 matrix phase.

Taran et al. conjectured that the origin for the improvement in electron emission was due to improved La diffusion mobility along the interface between the two phases compared to bulk LaB_6. This process resulted in excess La concentration at the surface of the cathode. Berger et al. recently showed that for the LaB_6–ZrB_2 eutectic enhanced emission around the phase boundaries was evident in ThEEM [35]. Diffusion at the phase boundaries is a likely mechanism for the observed emission enhancement. It was shown that by replacing ZrB_2 with a solid solution of (Zr, Ti)B_2 the emission activity decreased [11]. This was partially attributed to the presence of Ti atoms at the phase boundary interface. The solid solution di-boride is thought to form a more perfect interface, limiting the diffusion of La. Fig. 2(a), (b) show a LEEM image of the LaB_6–VB_2 surface with corresponding work function map. It can be seen in Fig 3(b) that low work function areas are primarily concentrated around the phase boundary between the two materials, with values ~1.6 eV. It should be noted that the surface cleaning procedure involves multiple high temperature flashes to 1250 °C. It is possible that the cleaning procedure promoted diffusion of La to

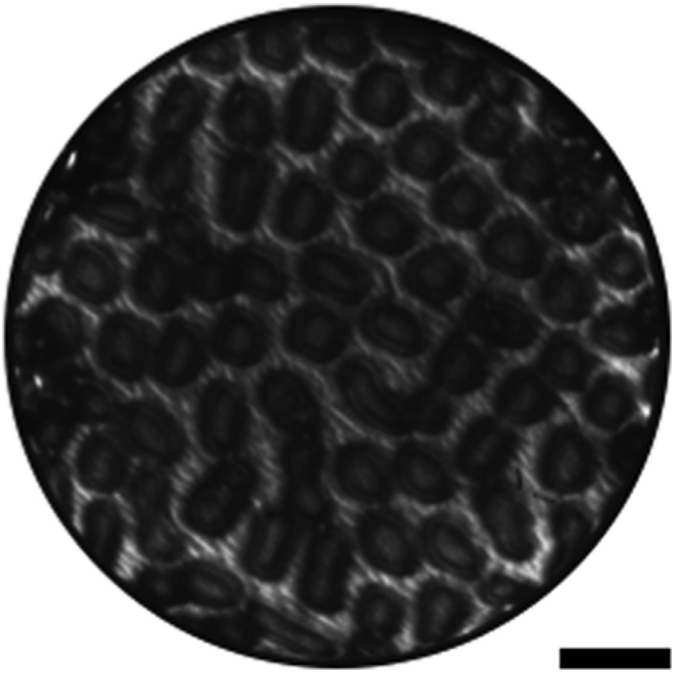

Fig. 2. LEEM image of LaB_6/VB_2 surface, electron landing energy 2 eV. The eutectic consist of a LaB_6 matrix with VB_2 rods. The rods are typically ~600 nm in diameter. Scale bar is 1 μm.

the surface of the eutectic similar to an effect previously shown with LaB_6–ZrB_2 [35].

A similar result was obtained with ThEEM. Fig 4(a) shows a ThEEM image at 977 °C. Most of the intensity in the image is concentrated on the VB_2 phase. Fig. 4(b) shows a thermionic emission curve generated from image intensity at various temperatures. Using the Richardson–Dushman equation [36], $I=AT^2exp-(\varphi/kT)$, where A is a material specific constant, T is temperature, φ is the work function and k is the Boltzmann's constant. We note that since we use image intensity and not the true current density in the Richardson–Dushman equation, no useful comparisons can be made with previously reported values for this constant. In this imaging mode the dominant physical property that contributes to image contrast is work function. Low work function areas will appear brighter. This is somewhat contradictory to the work function map in Fig 2(b), which showed the VB_2 phase to have similar work function as the LaB_6 matrix. The origin of this discrepancy is unknown at this time. The fact that the work function observed in the map and one calculated with the Richardson–Dushman equation are nearly identical indicates the origin of the work function are possibly the same. Given the large temperature difference, surface diffusion is likely to play a role in the emission activity shift from phase boundaries at room temperature to the primarily the VB_2 at 977 °C.

Although the SPLEEM is capable of heating the samples to temperatures that are typical of a working thermionic emitter, imaging at those conditions for extended periods of time is challenging for many reasons including detrimental *e*-beam heating of the objective lens and drift. Previous work involved thermionic emission experiments that exceeded 100 h [11]. However, simulating the effects of changes in stoichiometry by dosing the surface is quite easy in the SPLEEM. To do this La, V, and B were dosed separately on the surface, to roughly 1 ML coverage, by *e*-beam and thermal evaporation during image acquisition at room temperature. Fig. 5(a), (b), (c) shows the results of the dosing experiments. From B dosing results shown in Fig 4(a) it can be seen that the matrix has a significantly higher work function than the VB_2 phase. Higher work functions are also observed around the phase boundaries. This agrees well with the ThEEM image shown in Fig 4(a), which showed the primary emission areas to be on the VB_2 phase. La dosing shown in Fig 5(b) yielded low work function areas that were centered around the VB_2 phase. The V dosing shown if Fig 5(c) showed the most significant change in work function. Work functions as low as 1.1 eV were observed on the surface.

Qualitatively, the work function maps in Fig. 5 indicate an overall increase in the work with excess boron and decrease with excess La and V. It is apparent from the maps that V yielded the lowest work function change with values as low 1.1 eV. This suggest that La diffusion may not play a role in thermionic emission under these experimental conditions. It should be noted that previous thermionic emission experiments were conducted at temperatures much greater than 1000 °C. The work function analysis and thermionic emission imaging presented in this work represents emission characteristics well below that regime.

4. Summary

The work function of the LaB_6–VB_2 DSE was characterized through analysis of reflectivity curves acquired in the LEEM and ThEEM. At room temperature, low work function areas were observed around the phase boundaries. Previous work would suggest that these areas were the result of La diffusion. However, for the first time it was shown through ThEEM and elemental dosing that

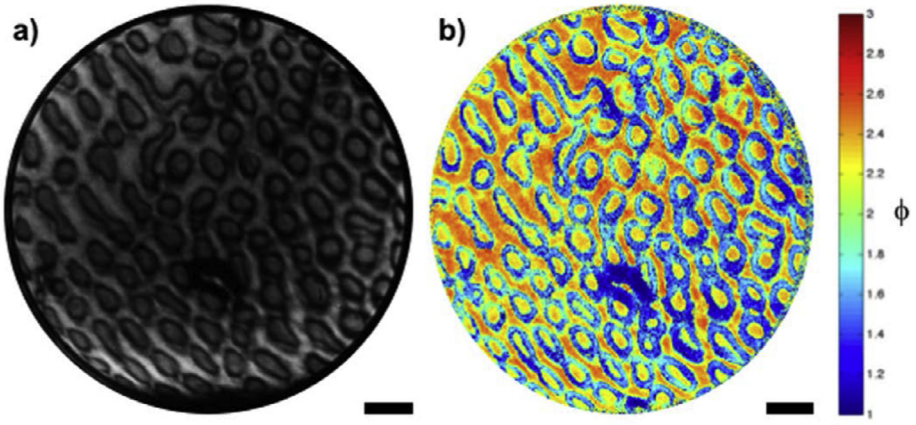

Fig. 3. (a) LEEM image of LaB_6/VB_2 surface, electron landing energy 1.1 eV; b) work function map created from a). Most of the low work function areas are concentrated around the phase boundaries between the LaB_6 (matrix) and the VB_2 (rods). Scale bar is 1 μm for both images.

Please cite this article as: T.C. Back et al., Work function characterization of directionally solidified LaB6–VB2 eutectic, Ultramicroscopy (2017), http://dx.doi.org/10.1016/j.ultramic.2017.05.006

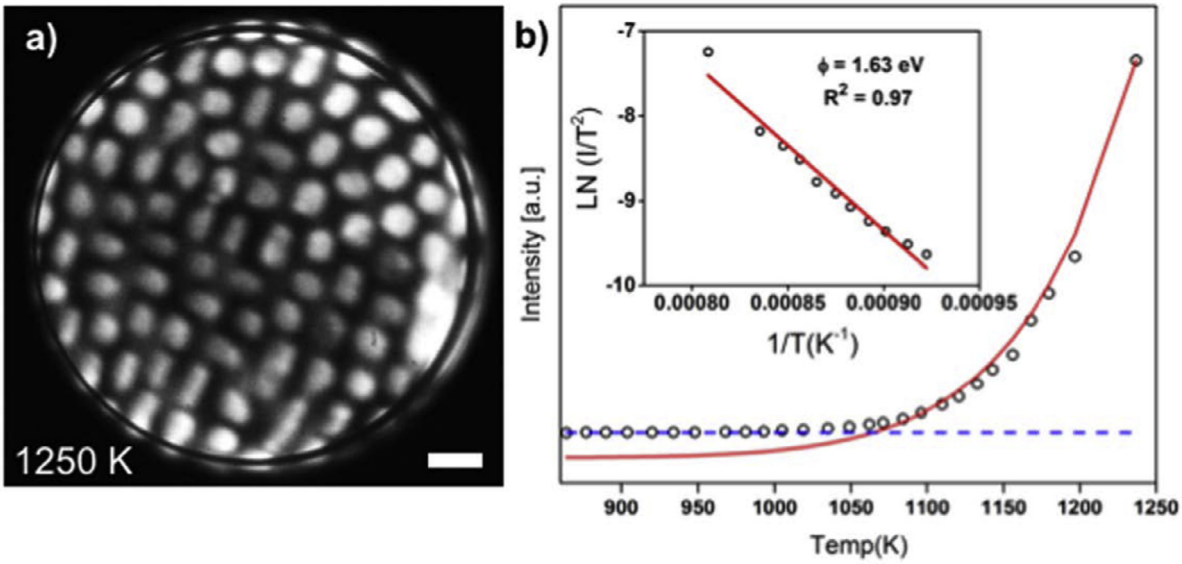

Fig. 4. (a) ThEEM image of LaB_6/VB_2 at 1250 K. Most of the intensity in the image is on or near the VB_2 phase. Scale bar is 1 μm. b) Thermionic emission curve generated from ThEEM images. A work function of 1.63 eV was calculated using the Richardson–Dushman equation. Blue dotted line indicates minimum value for integrated intensity on the detector. None of the points below this line were used for the calculation with the Richardson–Dushman equation. (For interpretation of the references to color in this figure legend, the reader is referred to the web version of this article.)

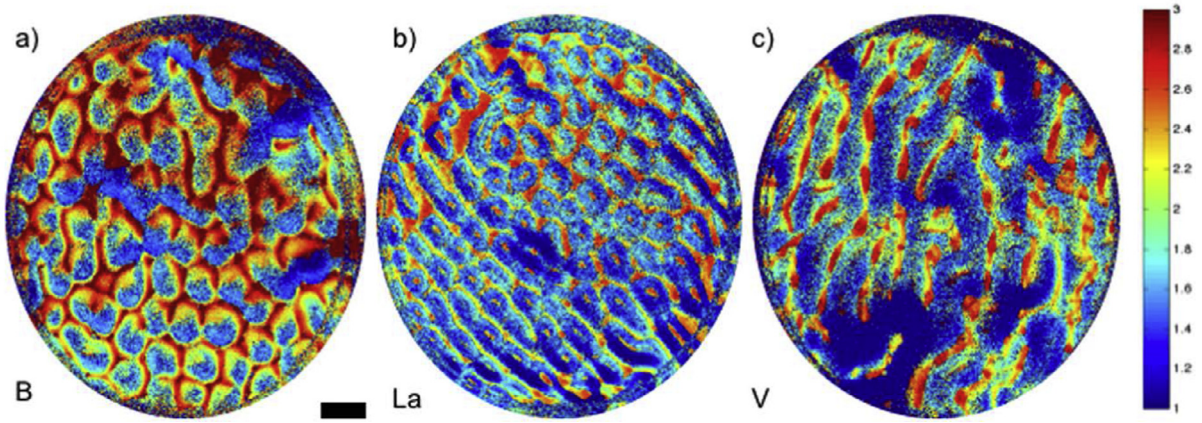

Fig. 5. 1 ML depositions of a) B, b) La, and c) V. The B deposition showed an overall increase in the work function while both the La and V deposition showed decrease. The scale bar is 1 μm and is applicable to all images.

vanadium may be responsible for the observed low work function areas, as low as 1.1 eV, at least in the low temperature, <1000 °C, regime.

Acknowledgments

TCB gratefully acknowledges support from U.S. Air Force Office of Scientific Research (grant no. FA8650-16-D-5403). Work at the Molecular Foundry was supported by the Office of Science, Office of Basic Energy Sciences, of the U.S. Department of Energy under Contract No. DE-AC02-05CH11231.

References

[1] J.M. Lafferty, Boride Cathodes, J. Appl. Phys. 22 (1951) 299–309.
[2] D.B. Williams, C.B. Carter, Transmission Electron Microscopy I Basics, Plenum Press, New York, New York, 1996.
[3] H. Deng, E.C. Dickey, Y. Paderno, V. Paderno, V. Filippov, Interface crystallography and structure in LaB6–ZrB2 directionally solidified eutectics, J. Am. Ceram. Soc. 90 (2007) 2603–2609.
[4] E.C. Dickey, V.P. Dravid, P.D. Nellist, D.J. Wallis, S.J. Pennycook, Three-dimensional atomic structure of NiO–ZrO2(cubic) interfaces, Acta Mater. 46 (1998) 1801–1816.
[5] V.P. Dravid, C.E. Lyman, M.R. Notis, A. Revcolevschi, Low-energy interfaces in NiO-ZrO2(CaO) eutectic, Metall. Trans. A 21 (1990) 2309–2315.
[6] R.S. Hay, Orientation relationships between complex low symmetry oxides: geometric criteria and interface structure for yttrium aluminate eutectics, Acta Mater. 55 (2007) 991–1007.
[7] R.S. Hay, L.E. Matson, Alumina/yttrium-aluminum garnet crystallographic orientation relationships and interphase boundaries: observations and interpretation by geometric criteria, Acta Metall. Mater. 39 (1991) 1981–1994.
[8] L. Mazerolles, D. Michel, R. Portier, Interfaces in oriented Al2O3-ZrO2 (Y2O3) eutectics, J. Am. Ceram. Soc. 69 (1986) 252–255.
[9] A. Sayir, S.C. Farmer, The effect of the microstructure on mechanical properties of directionally solidified Al2O3/ZrO2(Y2O3) eutectic, Acta Mater. 48 (2000) 4691–4697.
[10] Y.B. Paderno, V.N. Paderno, V.B. Filippov, Y.V. Mil'man, A.N. Martynenko, Structure features of the eutectic alloys of borides with the D- and f-transition metals, Soviet Powder Metallur. Metal Ceramics 31 (1992) 700–706.
[11] Y.B. Paderno, A.A. Taran, D.A. Voronovich, V.N. Paderno, V.B. Filipov, Thermionic properties of LaB6-(Ti 0.6 Zr 0.4)B2 material, Funct. Mater. 15 (2008) 63–67.
[12] A. Taran, D. Voronovich, S. Plankovskyy, V. Paderno, V. Filipov, Review of LaB6, Re-W dispenser, and BaHfO3-W cathode development, IEEE Trans. Electron Devices 56 (2009) 812–817.
[13] D.M. Goebel, E. Chu, High current lanthanum hexaboride hollow cathodes for high power hall thrusters, 32nd International Electric Propulsion Conference, Weisbaden, Germany, 2011.
[14] K. Grzelakowski, T. Duden, E. Bauer, H. Poppa, S. Chiang, A new surface microscope for magnetic imaging, IEEE Trans. Magn. 30 (1994) 4500–4502.

[15] T. Duden, E. Bauer, Spin-polarized low energy electron microscopy, Surf. Rev. Lett. 05 (1998) 1213–1219.
[16] B. Ünal, Y. Sato, K.F. McCarty, N.C. Bartelt, T. Duden, C.J. Jenks, A.K. Schmid, P.A. Thiel, Work function of a quasicrystal surface: icosahedral Al–Pd–Mn, J. Vacuum Sci. Technol. A 27 (2009) 1249–1250.
[17] M.L. Anderson, C.Y. Nakakura, G.L. Kellogg, Imaging doped silicon test structures using low energy electron microscopy, in, Sandia National Laboratory, 2010. http://prod.sandia.gov/techlib/access-control.cgi/2009/097981.pdf.
[18] M. Babout, J.C.L. Bosse, J. Lopez, R. Gauthier, C. Guittard, Mirror electron microscopy applied to the determination of the total electron reflection coefficient at a metallic surface, J. Phys. D: Appl. Phys. 10 (1977) 2331.
[19] M. Babout, C. Guittard, M. Guivarch, R. Pantel, M. Bujor, Mirror electron microscopy applied to the continuous local measurement of work-function variations, J. Phys. D: Appl. Phys. 13 (1980) 1161.
[20] C. Mathieu, N. Barrett, J. Rault, Y.Y. Mi, B. Zhang, W.A. de Heer, C. Berger, E.H. Conrad, O. Renault, Microscopic correlation between chemical and electronic states in epitaxial graphene on SiC$(000\overline{1})$, Phys. Rev. B 83 (2011) 235436.
[21] H.S. Mok, A. Ebnonnasir, Y. Murata, S. Nie, K.F. McCarty, C.V. Ciobanu, S. Kodambaka, Kinetics of monolayer graphene growth by segregation on Pd(111), Appl. Phys. Lett. 104 (2014) 101606 (101604 pp.).
[22] R. Claessen, H. Carstensen, M. Skibowski, Conduction-band structure of graphite single crystals studied by angle-resolved inverse photoemission and target-current spectroscopy, Phys. Rev. B 38 (1988) 12582–12588.
[23] A.R. Law, J.J. Barry, H.P. Hughes, Angle-resolved photoemission and secondary electron emission from single-crystal graphite, Phys. Rev. B 28 (1983) 5332–5335.
[24] D. Neumann, G. Meister, U. Kürpick, A. Goldmann, J. Roth, V. Dose, Interaction of atomic hydrogen with the graphite single-crystal surface, Appl. Phys. A 55 (1992) 489–492.
[25] T. Takahashi, H. Tokailin, T. Sagawa, Angle-resolved ultraviolet photoelectron spectroscopy of the unoccupied band structure of graphite, Phys. Rev. B 32 (1985) 8317–8324.
[26] R.F. Willis, B. Fitton, G.S. Painter, Secondary-electron emission spectroscopy and the observation of high-energy excited states in graphite: theory and experiment, Phys. Rev. B 9 (1974) 1926–1937.
[27] K. Besocke, B. Krahl-Urban, H. Wagner, Dipole moments associated with edge atoms; a comparative study on stepped Pt, Au and W surfaces, Surf. Sci. 68 (1977) 39–46.
[28] M.A. Gleeson, K. Mårtensson, B. Kasemo, D.V. Chakarov, Co-adsorption and reactions of Na and H2O on graphite, Appl. Surf. Sci. 235 (2004) 91–96.
[29] B. Krahl-Urban, E.A. Niekisch, H. Wagner, Work function of stepped tungsten single crystal surfaces, Surf. Sci. 64 (1977) 52–68.
[30] R.W. Strayer, W. Mackie, L.W. Swanson, Work function measurements by the field emission retarding potential method, Surf. Sci. 34 (1973) 225–248.
[31] L. van Someren, Work function measurements on macroscopic tungsten specimens, Surf. Sci. 20 (1970) 221–234.
[32] Y. Yamamoto, T. Miyokawa, Emission characteristics of a conical field emission gun, journal of vacuum science & technology B: microelectronics and nanometer structures processing, Measure. Phenom. 16 (1998) 2871–2875.
[33] E. Starodub, N.C. Bartelt, K.F. McCarty, Viable thermionic emission from graphene-covered metals, Appl. Phys. Lett. 100 (2012) 181604.
[34] Y.B. Paderno, A.A. Taran, E.K. Ostrovski, V.N. Paderno, V. Filippov, Manufacturing, structure and thermionic properties of lanthanum hexaboride based composite cathode materials, Funct. Mater. 8 (2001) 714–717.
[35] M.-H. Berger, T.C. Back, P. Soukiassian, D. Martinotti, L. Douillard, S.B. Fairchild, J.J. Boeckl, V. Filipov, J. Mater. Sci. (2016) Accepted.
[36] S. Dushman, Thermionic emission„ Rev. Mod. Phys. 2 (1930) 381–476.

Please cite this article as: T.C. Back et al., Work function characterization of directionally solidified LaB6–VB2 eutectic, Ultramicroscopy (2017), http://dx.doi.org/10.1016/j.ultramic.2017.05.006